

1 ***Supplement of***

2 **Pivotal role of the North African Dipole Intensity (NAFDI) on**
3 **alternate Saharan dust export over the North Atlantic and**
4 **the Mediterranean, and relationship with the Saharan Heat**
5 **Low and mid-latitude Rossby waves**

6

7 **E. Cuevas¹, A. J. Gómez-Peláez¹, S. Rodríguez¹, E. Terradellas², S. Basart³, R.**
8 **D. García^{1,4}, O. E. García¹ and S. Alonso-Pérez⁵**

9 [1] {Izaña Atmospheric Research Centre (AEMET), Santa Cruz de Tenerife, Spain}

10 [2] {SDS-WAS Regional Centre (AEMET), Barcelona, Spain}

11 [3] {Earth Sciences Department, Barcelona Supercomputing Centre, Barcelona, Spain}

12 [4] {Air Liquide S.A., Delegación de Canarias, Candelaria, Santa Cruz de Tenerife, Spain}

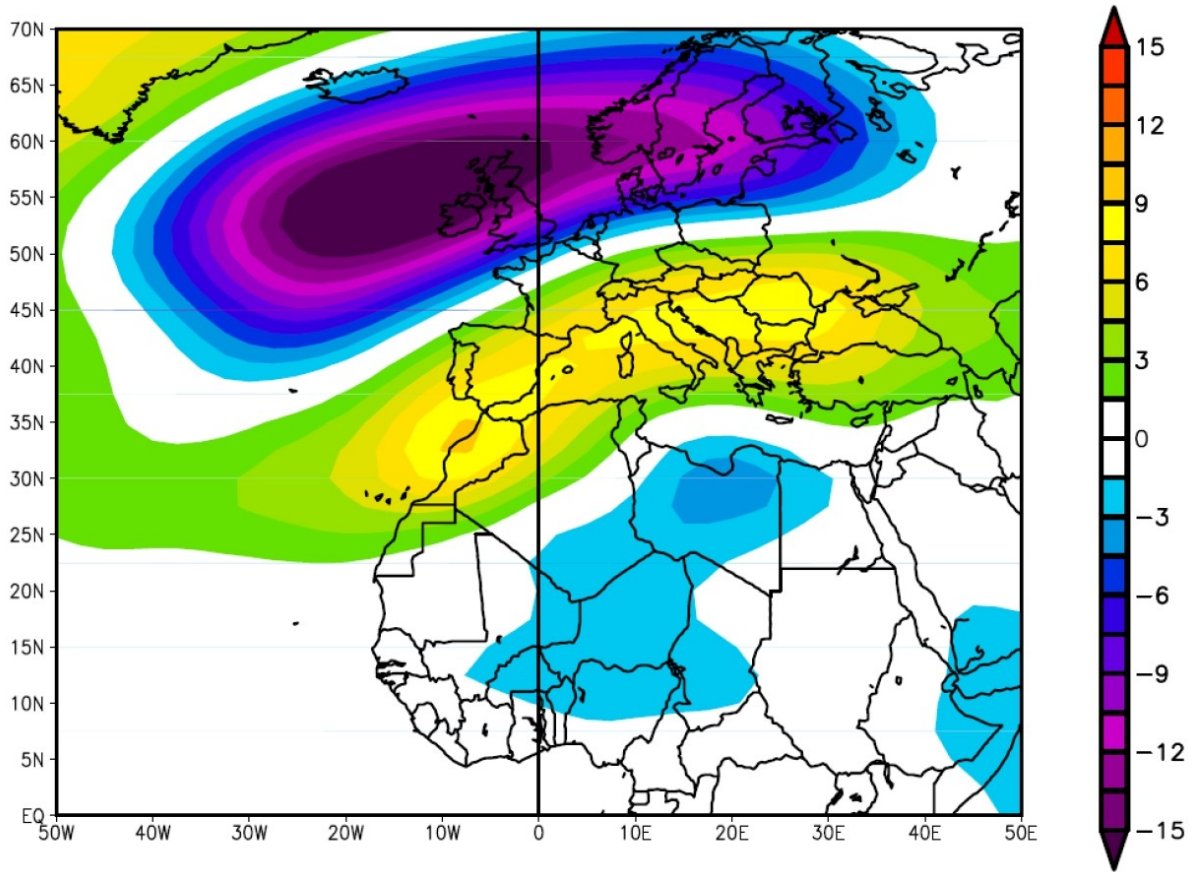
13 [5] {Universidad Europea de Canarias, La Orotava, Santa Cruz de Tenerife, Spain}

14

15

1 **S1. Associated regression plot to the correlation plots of Figure 1.**

2



3

4 Figure S1. NCEP monthly regression plot between the revised NAFDI and the geopotential
5 height at 700 hPa for August months for the period 1980-2013.

6

7

8

9

10

11

12

1 **S2. NAFDI values corresponding to June, July and August for each year of the**
2 **period 2003-2012.**

3

	Jun	Jul	Aug
2003	1.0513	0.9276	-0.2049
2004	0.6771	0.0567	-0.7104
2005	1.3763	-0.6829	-0.2388
2006	-0.4246	0.7543	-1.5468
2007	-1.6420	0.8123	-1.1226
2008	0.1713	0.0841	1.0161
2009	0.7721	1.3567	-0.3572
2010	-3.0921	0.3913	0.5185
2011	1.0197	-1.2401	0.2967
2012	2.2938	1.494	2.2919

NAFDI > +0.4

NAFDI < -0.4

-0.4 < NAFDI < +0.4

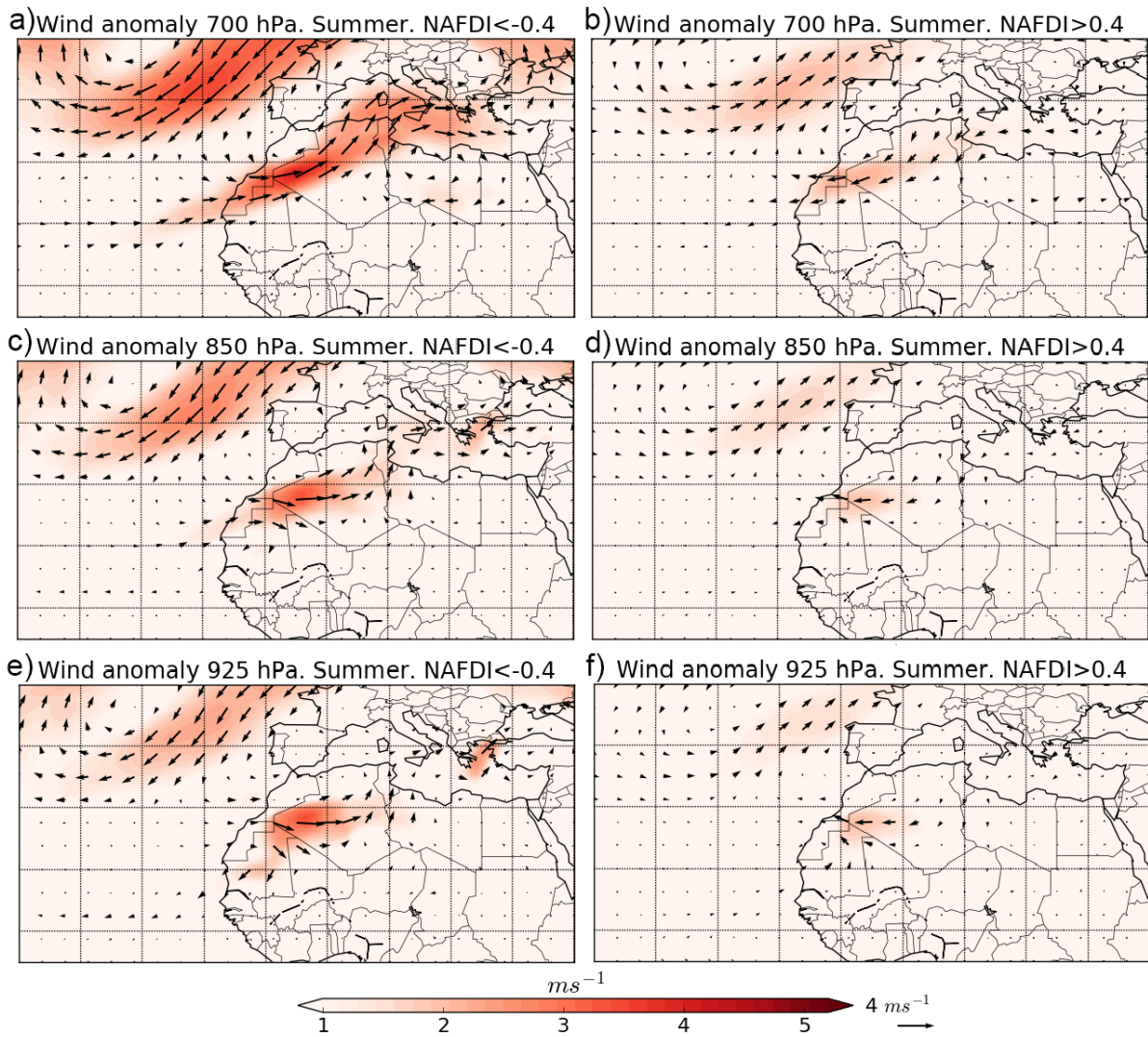
4

5 Table S2. Monthly-mean NAFDI values corresponding to June, July and August for each year
6 of the period 2003-2012. In blue and red are marked The selected months selected to group
7 AOD and meteorological data during positive and negative NAFDI are marked in blue and
8 red, respectively.

9

1 **S3. Summer wind anomalies (700, 850 and 925 hPa) for negative and positive**
2 **NAFDI.**

3

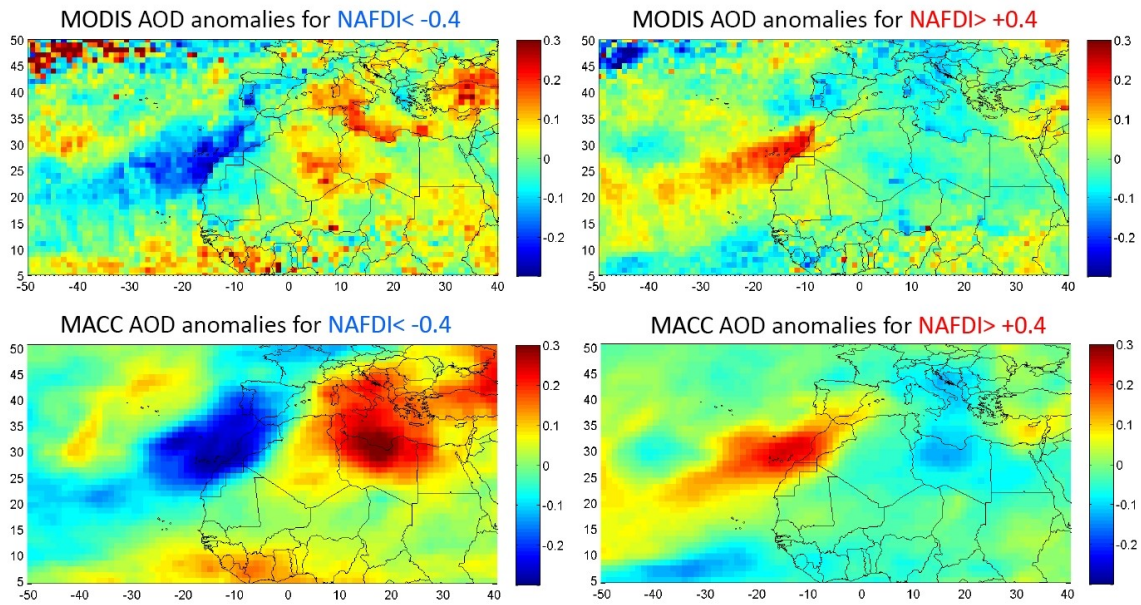


4
5

6 Figure S3. Monthly averages of ECMWF wind vector and speed anomalies for summer in the
7 period 2003-2012 at 700, 850 and 925 hPa, for positive and negative NAFDI phases.

8

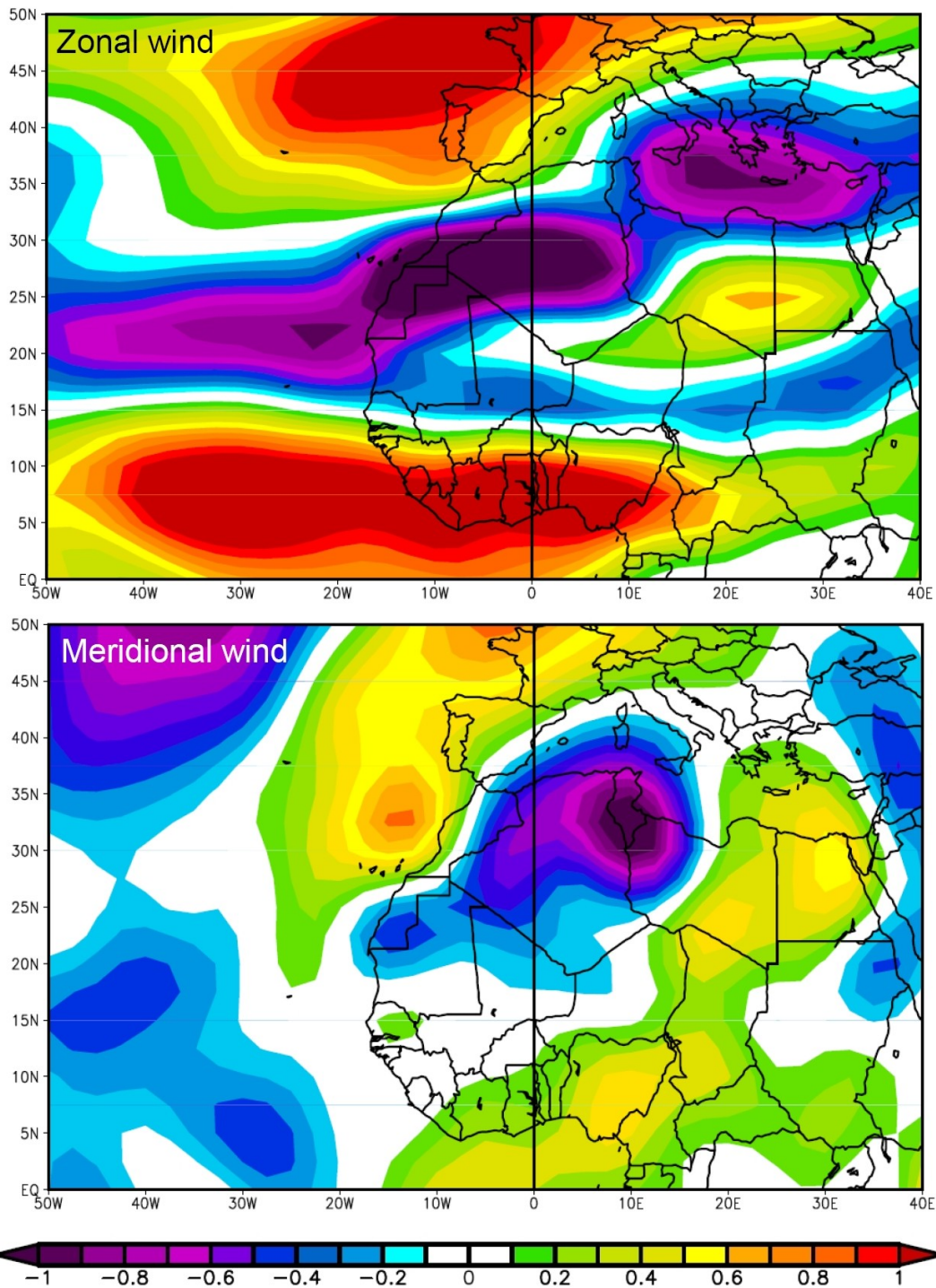
1 **S4. MODIS and MACC AOD anomalies in summer for negative and positive**
2 **NAFDI.**



3
4 Figure S4. Averaged AOD anomalies from MODIS and MACC in summer for positive and
5 negative NAFDI phases, within the period 2003-2012. These plots were obtained by
6 averaging the AOD anomalies for each month and each phase of the NAFDI (from MODIS
7 and MACC, respectively), and then calculating a weighted average of the anomalies for
8 summer period (June-August) for each phase of the NAFDI.

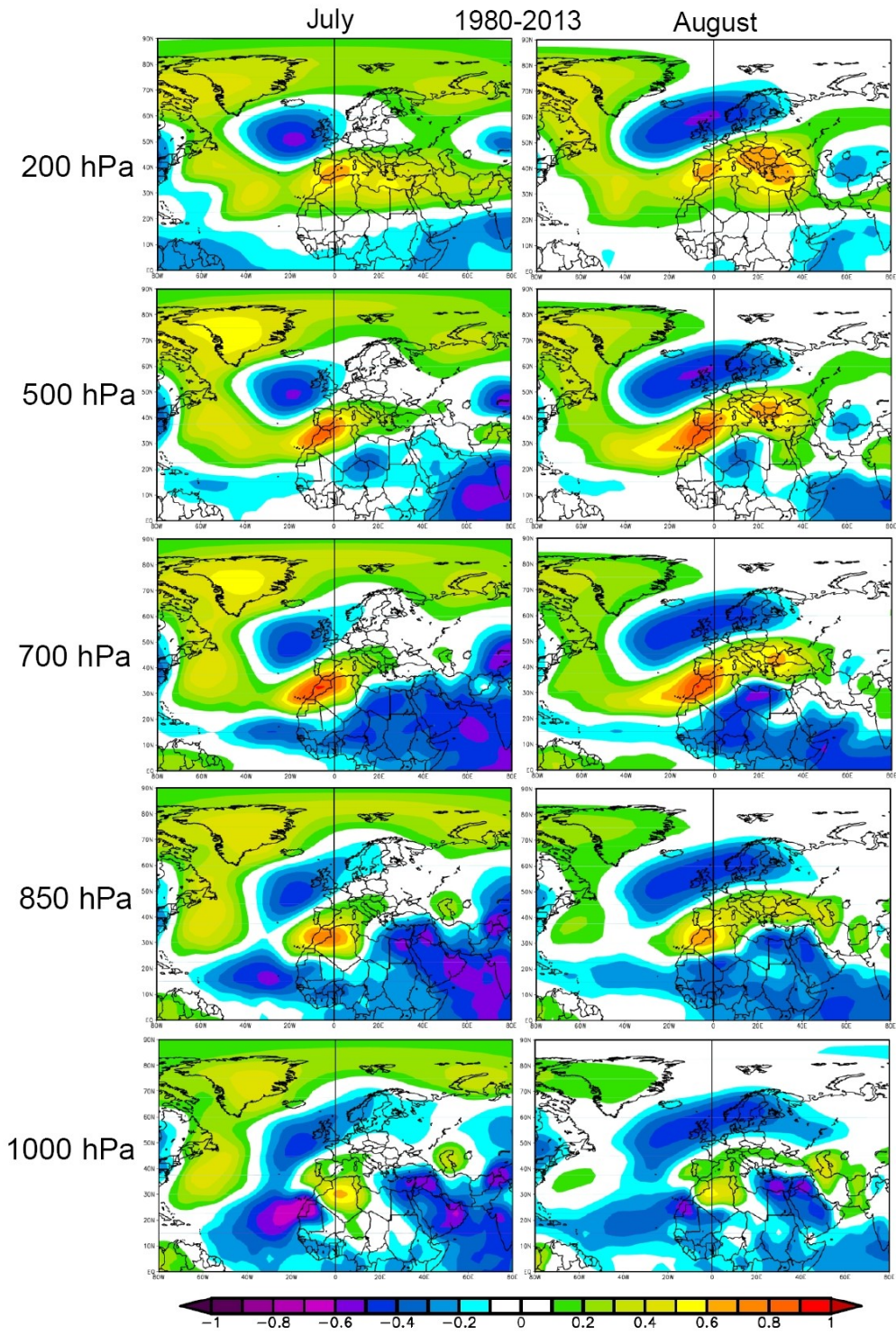
9
10

- 1 **S5. Regression plots between NAFDI and 700 hPa zonal (for the Atlantic) and**
- 2 **meridional (for the Mediterranean) wind components for the period 1980-2013.**



- 3
- 4 Figure S5. NCEP regression plots between NAFDI and 700 hPa zonal (for the Atlantic; upper
- 5 panel) and meridional (for the Mediterranean; lower panel) wind components for the period
- 6 1980-2013.

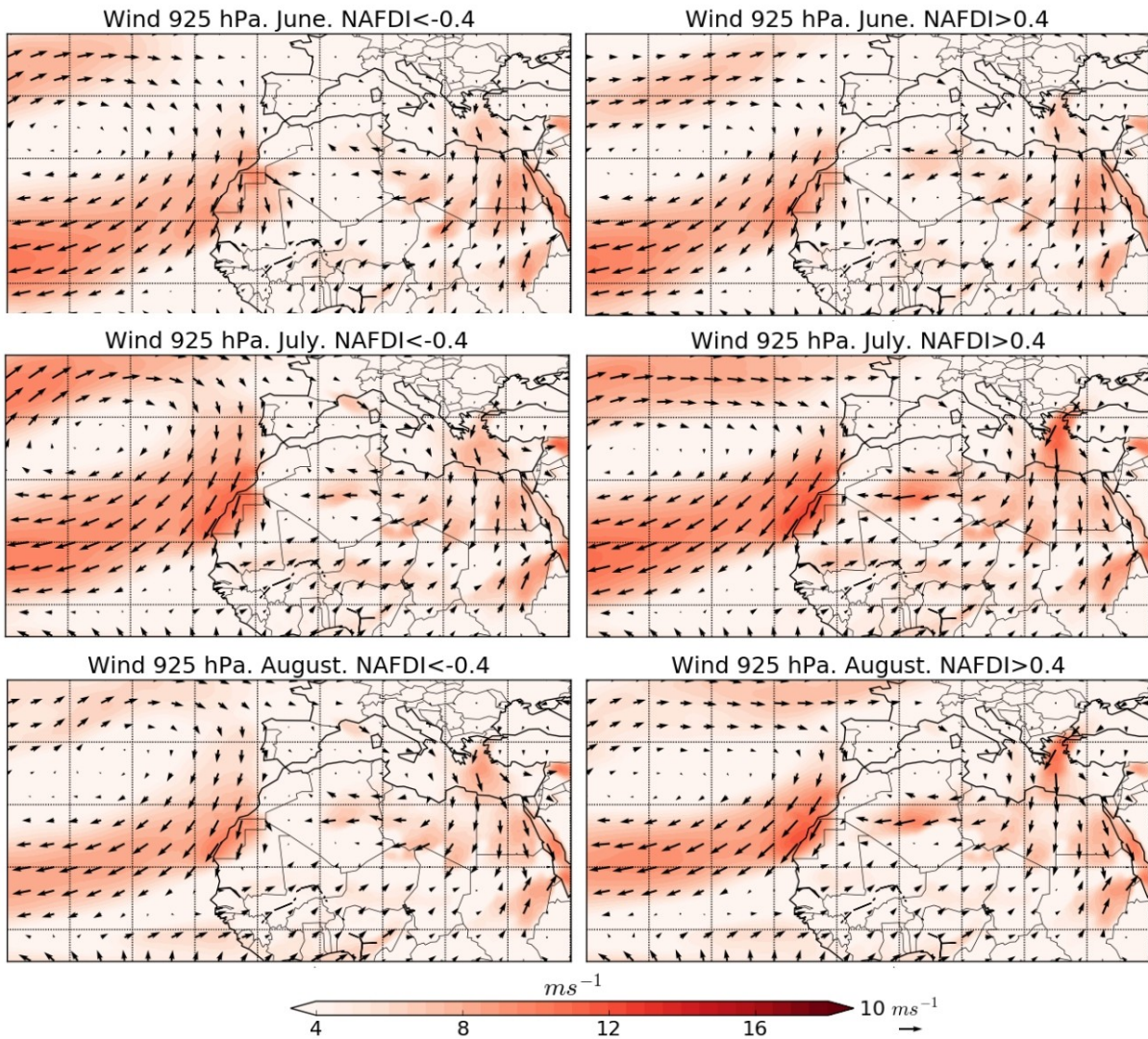
- 1 **S6. Correlation plots between NAFDI and 200, 500, 700, 850 and 1000 hPa**
- 2 **geopotential height in July and August, for the period 1980-2013.**



- 3
- 4 Figure S6. NCEP correlation plots between NAFDI and 200, 500, 700, 850 and 1000 hPa
- 5 geopotential heights in July (left column) and August (right column), for the period 1980-
- 6 2013.

1 **S7. Wind direction and speed at 925 hPa monthly averages for June, July and August**
2 **with positive and negative NAFDI phases, in the period 2003-2012.**

3



4

5 Figure S7. Monthly averages of ECMWF wind vector and speed at 925 hPa for summer
6 months (June, July and August) with positive and negative NAFDI phases, for the period
7 2003-2012.

8

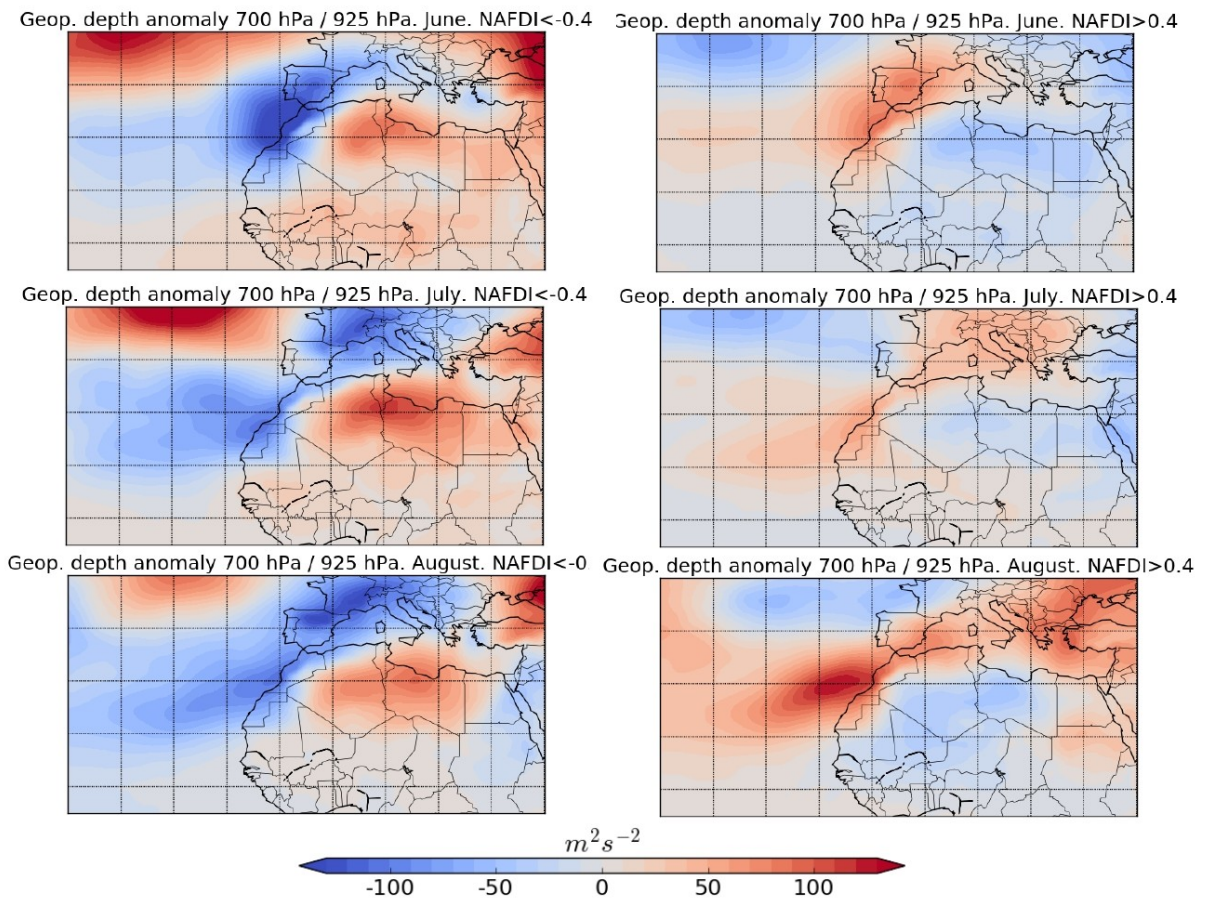
9

10

11

1 **S8. Geopotential 700-925 hPa depth anomalies for positive and negative NAFDI phases,**
2 **in the period 2003-2012.**

3



4

5 Figure S8. Monthly averages of ECMWF 700-925 hPa geopotential depth anomalies for June,
6 July and August, for positive and negative NAFDI phases, within the period 2003-2012.

7

1 **S9. Statistics pointing out the SHL is indeed more intense during its East**
 2 **phase, using a definition of SHL intensity equivalent to that of Lavaysse et al.**
 3 **(2010a).**

4 The geographical points used in the paper to define the daily SHLWEDI were selected using
 5 the locations of the maximum and minimum of the dipolar pattern that corresponds to the
 6 EOF of the SHL location obtained by Lavaysse et al. (2013) (see their Fig. 5c). Lavaysse et
 7 al. (2015) show in their Figure 1 the mean occurrence probability of the heat low detection
 8 during the summer season (20 June – 17 September) from 1979 to 2012 (using both LLAT
 9 and 850 hPa temperature). Based on that figure, we have selected the point 2.5°W, 25°N as
 10 having the maximum (or near the maximum) occurrence probability of SHL detection. As a
 11 rough proxy for the daily SHL intensity, we have used: 1) the mean 850 hPa temperature for
 12 the points 25°N, 12.5°W (Western centre of the mentioned dipolar pattern) and 2.5°W, 25°N
 13 (maximum probability of SHL detection), when the SHL is in West-phase; 2) the mean 850
 14 hPa temperature for the points 20°N, 7.5°E (Eastern centre of the dipolar pattern) and 2.5°W,
 15 25°N (maximum probability of SHL detection), when the SHL is in East-phase. For the
 16 period 1980-2013 20 June – 17 September, the mean SHL intensity (standard deviation) is: 1)
 17 300.9 K (1.54 K) when the SHL is in West-phase (SHLWEDI>0); and 2) 302.0 K (1.39 K)
 18 when the SHL is in East-phase (SHLWEDI<0). The following table shows statistics about the
 19 distribution frequency of the SHL intensities.

20

Condition	West phase	East phase
> 300 K	76.2%	91.5%
> 301 K	51.4%	77.9%
> 302 K	24.9%	51.2%
> 303 K	7.3%	26.0%
> 304 K	0.7%	7.0%
> 305 K	0.0%	0.5%

21 Table 1. Fraction of SHL West (East) phase days for which the indicated condition on the
 22 SHL intensity holds, for the period 1980-2013 20 June – 17 September. The total number of
 23 days with West-phase is 1773, whereas there are 1287 days with East-phase.

1

2 **S10 Analytical relations, equation that describes the Omega field associated to**
3 **the Rossby wave in terms of the Geisler and Dickinson (1975) eigenvector, and**
4 **empirical relation with the vertical shear of the zonal flow**

5 Geisler and Dickinson (1975) obtained solutions for external Rossby modes on a beta-plane
6 with realistic vertical wind shear. They assume an atmosphere isothermal in the vertical
7 direction but with a latitude-dependent temperature, $T_0(y)$. Therefore, they have thermal wind,
8 that is, an altitude-dependent zonal flow, $u_0(p)$. They use the log pressure coordinate
9 $z=\ln(p_r/p)$, where p_r is a reference pressure at the ground. However, for easiness of
10 presentation here, we are going to use the pressure as vertical coordinate except for the
11 function $\psi(z)$ that is introduced latter. They consider small perturbations to the background
12 flow in the form (we use geopotential instead of geopotential height):

13

$$\Phi'(x, y, z, t) = f_0 \left(\frac{p_r}{p} \right)^{1/2} \psi(z) \exp[i(kx + ly - \omega t)] \quad (\text{Equation S1}),$$

15

16 where the left hand side is the perturbed geopotential, f_0 is the Coriolis parameter at a
17 reference latitude, k is the longitudinal wavenumber, l is the latitudinal wavenumber, and ω is
18 the Eulerian angular frequency (i.e., they perform Fourier analysis in the latitudinal and
19 longitudinal coordinate as well as in time). In the absence of vertical shear of the background
20 zonal wind, the function $\psi(z)$ is equal to a constant. They introduce this form of the perturbed
21 geopotential into the perturbed quasi-geostrophic potential vorticity equation (considering
22 appropriate boundary conditions) and reduce the problem to an eigenvalue problem for the
23 eigenvector $\psi(z)$ with a set of two ordinary differential equations in z , which they solve
24 numerically.

25 From the perturbed geopotential height, all the perturbed variables can be obtained using the
26 quasi-geostrophic relations (e.g., Holton, 1992) in a straightforward way. For example, this is
27 the equation that holds for the perturbed zonal flow:

28

$$u'(x, y, z, t) = -il \left(\frac{p_r}{p} \right)^{1/2} \psi(z) \exp[i(kx + ly - \omega t)] \quad (\text{Equation S2})$$

30

1 Using the perturbed quasi-geostrophic energy equation (e.g., see Holton, 1992), we have
 2 obtained the following equation for the perturbed omega:

$$\omega'(x, y, z, t) = \frac{iR}{p\sigma(p)} \left[(u_0(p)k - kc) \frac{f_0}{R} \left(\frac{\psi(z)}{2} + \frac{\partial\psi(z)}{\partial z} \right) + k\psi(z) \frac{\partial T_0}{\partial y} \right] \left(\frac{p_r}{p} \right)^{1/2} \exp[i(kx + ly - kt)] \quad \text{(Equation S3),}$$

6 where R is the gas constant for dry air,

$$7 \quad \sigma(p) = -R \frac{T_0(y_0)}{p} \frac{d \ln \theta_0}{dp} \quad \text{(Equation S4),}$$

8 and θ_0 is the potential temperature of the unperturbed atmosphere. The thermal wind relation
 9 for the unperturbed atmosphere is given by:

$$10 \quad f_0 \frac{\partial u_0}{\partial p} = \frac{R}{p} \frac{\partial T_0}{\partial y} \quad \text{(Equation S5)}$$

11 In case there is no thermal wind (i.e., the zonal velocity is constant in pressure), $\psi(z)$
 12 becomes a constant, whereas for the external Rossby modes obtained by Geisler and
 13 Dickinson (1975) when there is thermal wind (see their Figure 10), $\psi(z)$ has a significant
 14 maximum in the lower, middle and/or upper troposphere. That is, the vertical shear of the
 15 zonal wind allows the free Rossby wave to have a very significant amplitude in the middle
 16 and lower troposphere. We expect from Eq. S3 that the perturbed omega at a given level will
 17 be very roughly proportional to the value of $\psi(z)$ at such level. Based on these results, we use
 18 in the paper the Omega at 500 hPa as a tracer of the capacity of the free barotropic Rossby
 19 wave to go deep in the lower troposphere. We use the term “go deep in the lower
 20 troposphere” because in the real atmosphere we expect the free Rossby waves to transport
 21 longitudinally their energy along the upper troposphere (the lower troposphere has a less
 22 zonal flow, i.e., it has a significant contribution of the meridional flow that changes a lot in
 23 longitude) and that the Rossby wave is noticed more or less in the lower troposphere
 24 depending on the vertical shear of the zonal wind. In the next paragraph, we prove
 25 numerically that this relation holds.

26 In order to test the relation between the amplitude of O500 (defined in Section 3.4 of the
 27 paper) and the vertical shear of the background zonal wind, we have obtained NCEP daily
 28 zonal wind time series at 2.5°E and 32.5°N for the levels 500 hPa (denoted as ZWB500) and

1 200 hPa (denoted as ZWB200). Since indeed we do not have the amplitude of O500 but its
2 instantaneous daily value, we compute the correlation using only days for which the absolute
3 value of the NAFDI is greater than a threshold (we expect the instantaneous value of O500
4 approaches the O500 amplitude as the threshold grows). In Supplement S15, we show the
5 mean zonal wind (averaged also in longitude from 10°W to 10°E) for a latitudinal-vertical
6 cross-section during the period July-August 1980-2013. In some sense, the ZWB200 value is
7 by itself representative of the mean vertical shear of the background zonal wind, due to the
8 fact that the wind speed is much smaller near the ground than at 200 hPa. The correlation
9 between the daily ZWB200 and O500 time series for days in which the absolute value of the
10 NAFDI is larger than 1.3, is 0.251; whereas if the NAFDI threshold is set at 2.6 (3.9) the
11 correlation becomes 0.297 (0.335). These correlation values do not decrease significantly if a
12 15-day or 29-day running mean is applied previously to the ZWB200 time series. The
13 correlations of the time series ZWB200 minus ZWB500, with O500 are smaller but
14 significant (e.g., 0.194 for a NAFDI threshold of 3.9).

15 However, to describe in a more accurate way the propagation of these Rossby waves in the
16 real atmosphere, a much more sophisticated (and difficult) mathematical model would be
17 necessary (not done in the literature according to our knowledge): a background zonal flow
18 depending “strongly” in latitude and height, and depending “slightly” in longitude. The
19 perturbation problem for such background flow would lead to an eigenvalue problem with
20 Partial Differential Equations depending on latitude and height simultaneously, combined
21 with a WKB method in the longitudinal direction and Fourier analysis in time.

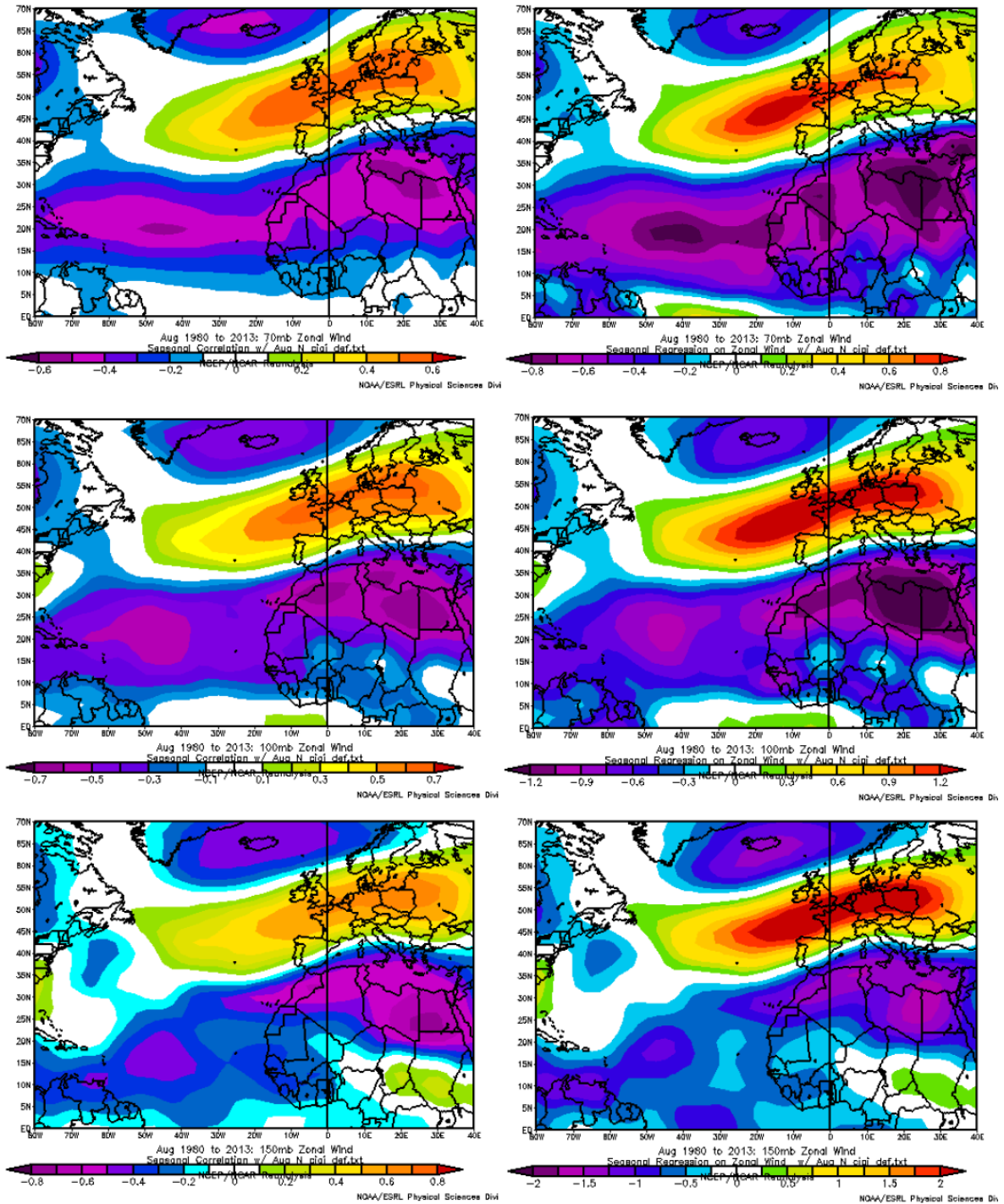
22

23

1 **S11. NCEP monthly correlation and regression maps between the monthly**
2 **NAFDI for August months of the period 1980-2013 and the zonal wind,**
3 **meridional wind, or omega.**

4

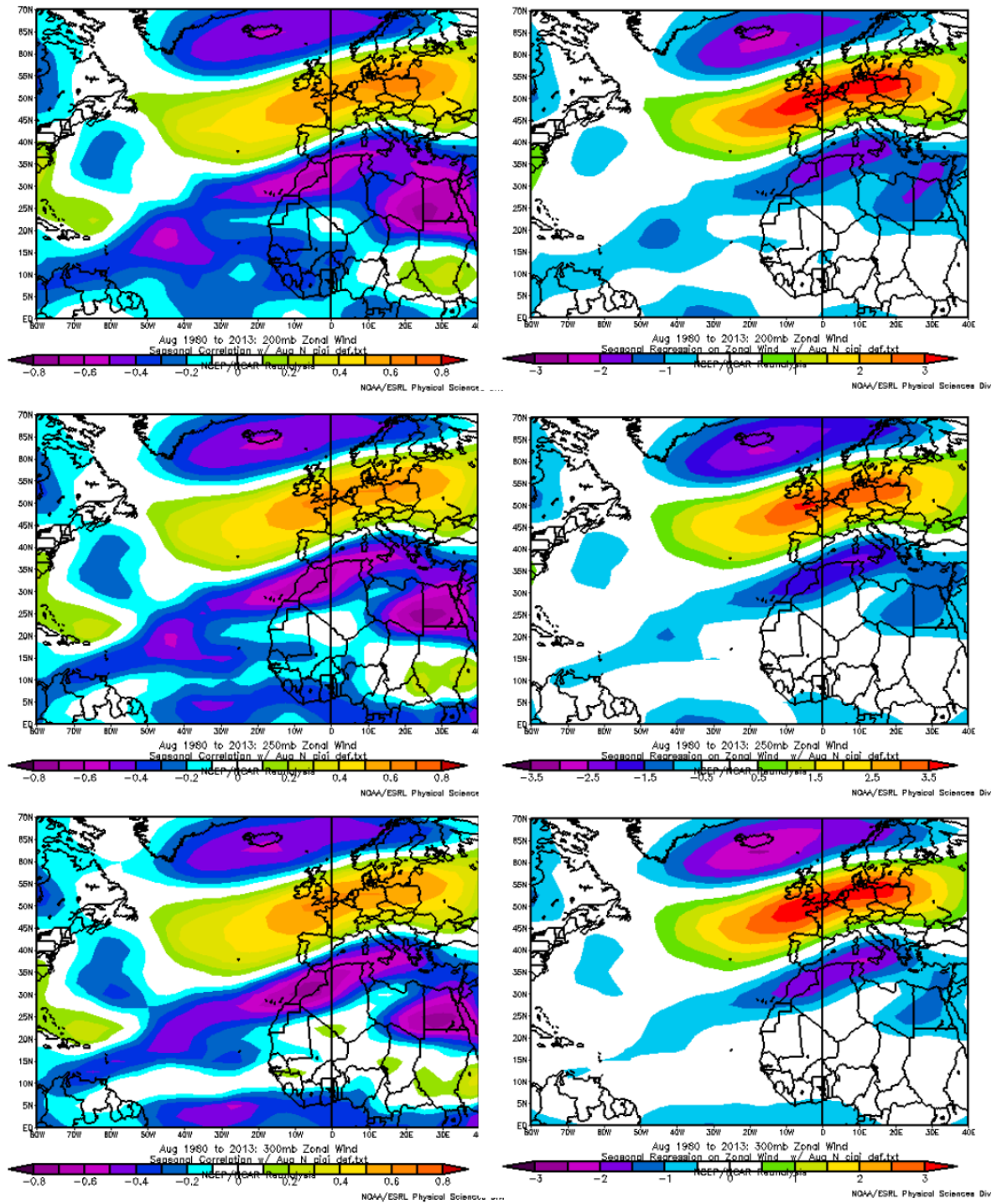
1



2

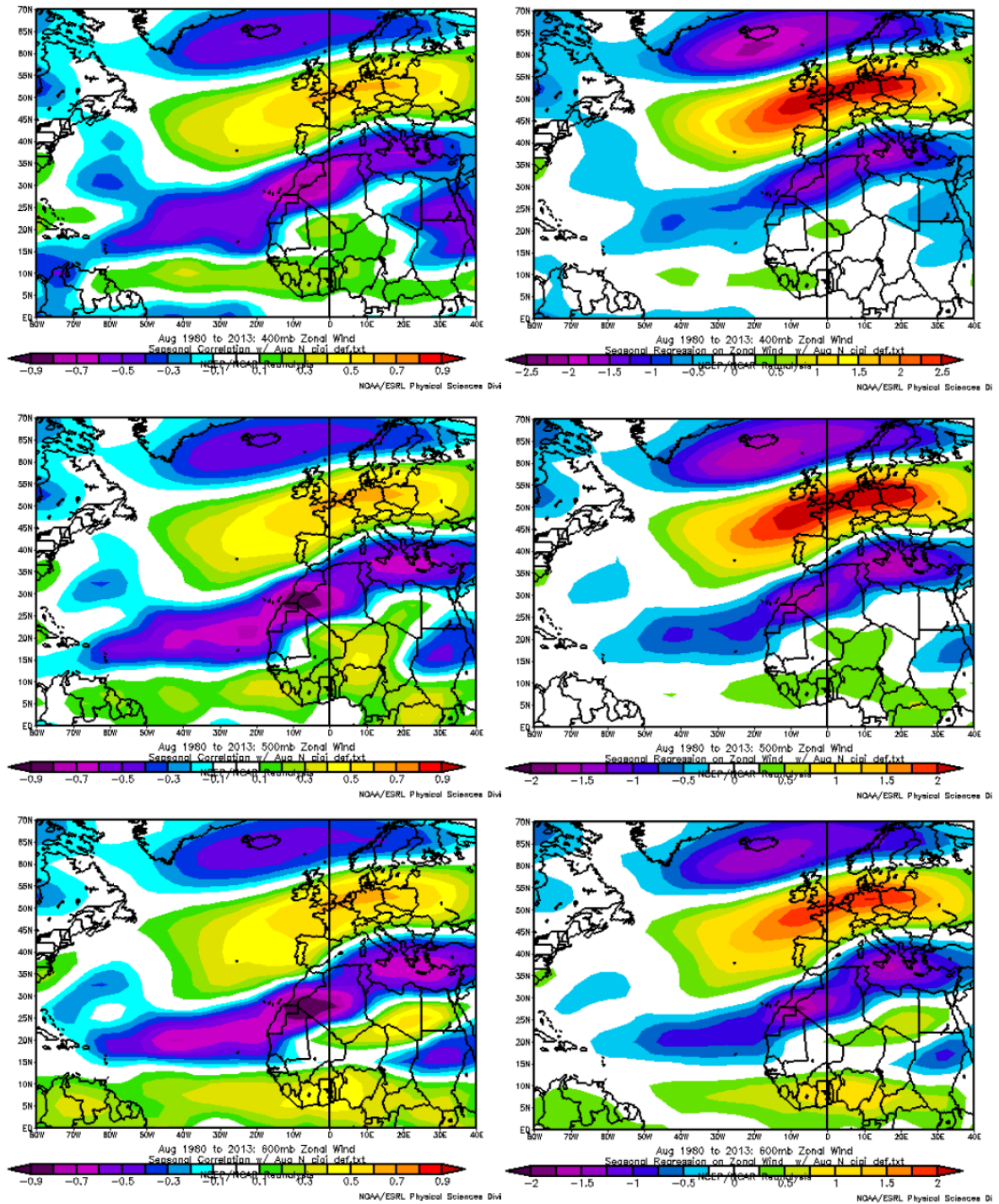
3 Figure S11-1. NCEP monthly correlation and regression plots between the zonal wind at
4 different pressure levels (70, 100 and 150 hPa) and the monthly NAFDI for August months of
5 the period 1980-2013.

6



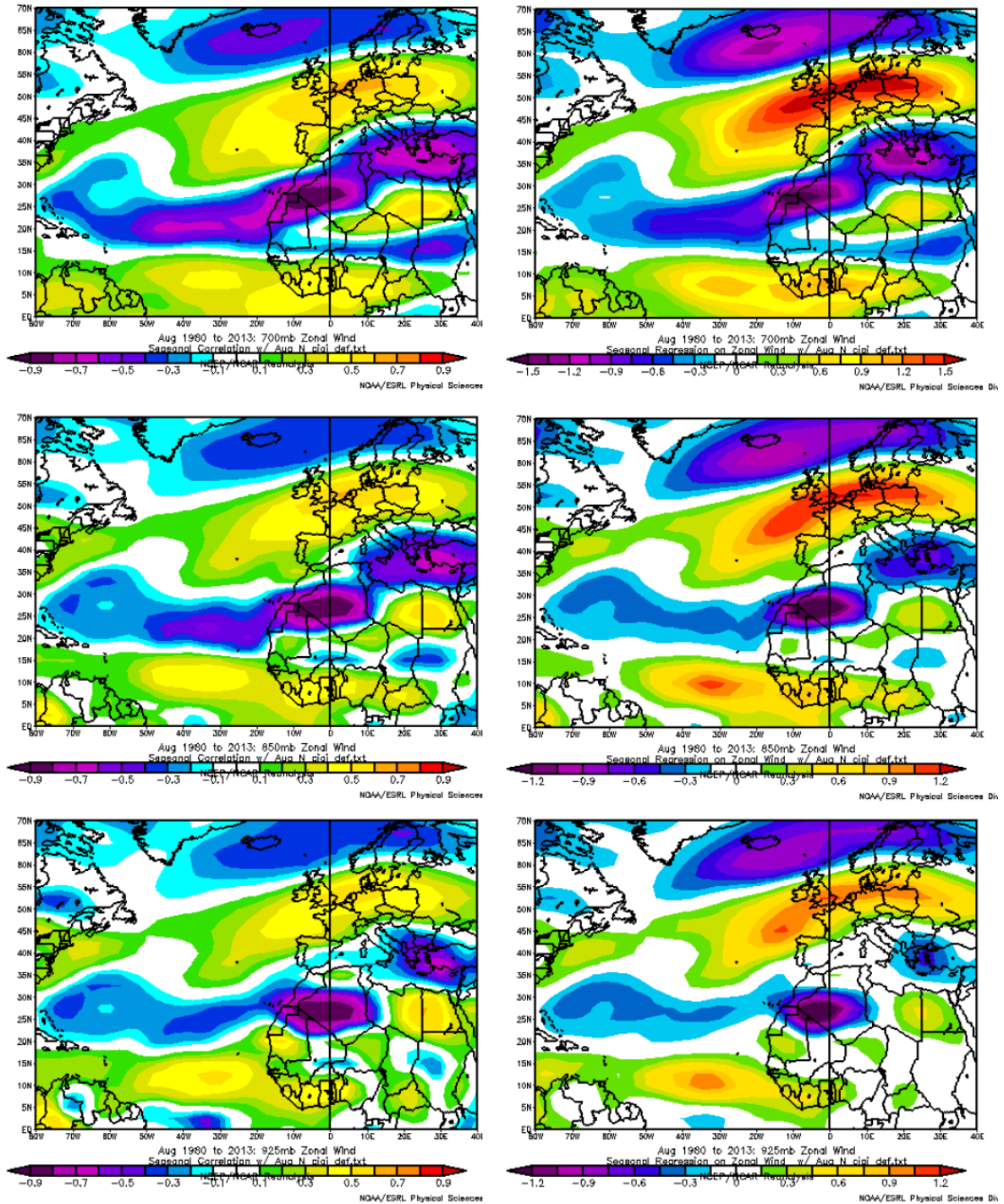
1
 2 Figure S11-2. NCEP monthly correlation and regression plots between the zonal wind at
 3 different pressure levels (200, 250 and 300 hPa) and the monthly NAFDI for August months
 4 of the period 1980-2013.

5



1
2
3
4
5

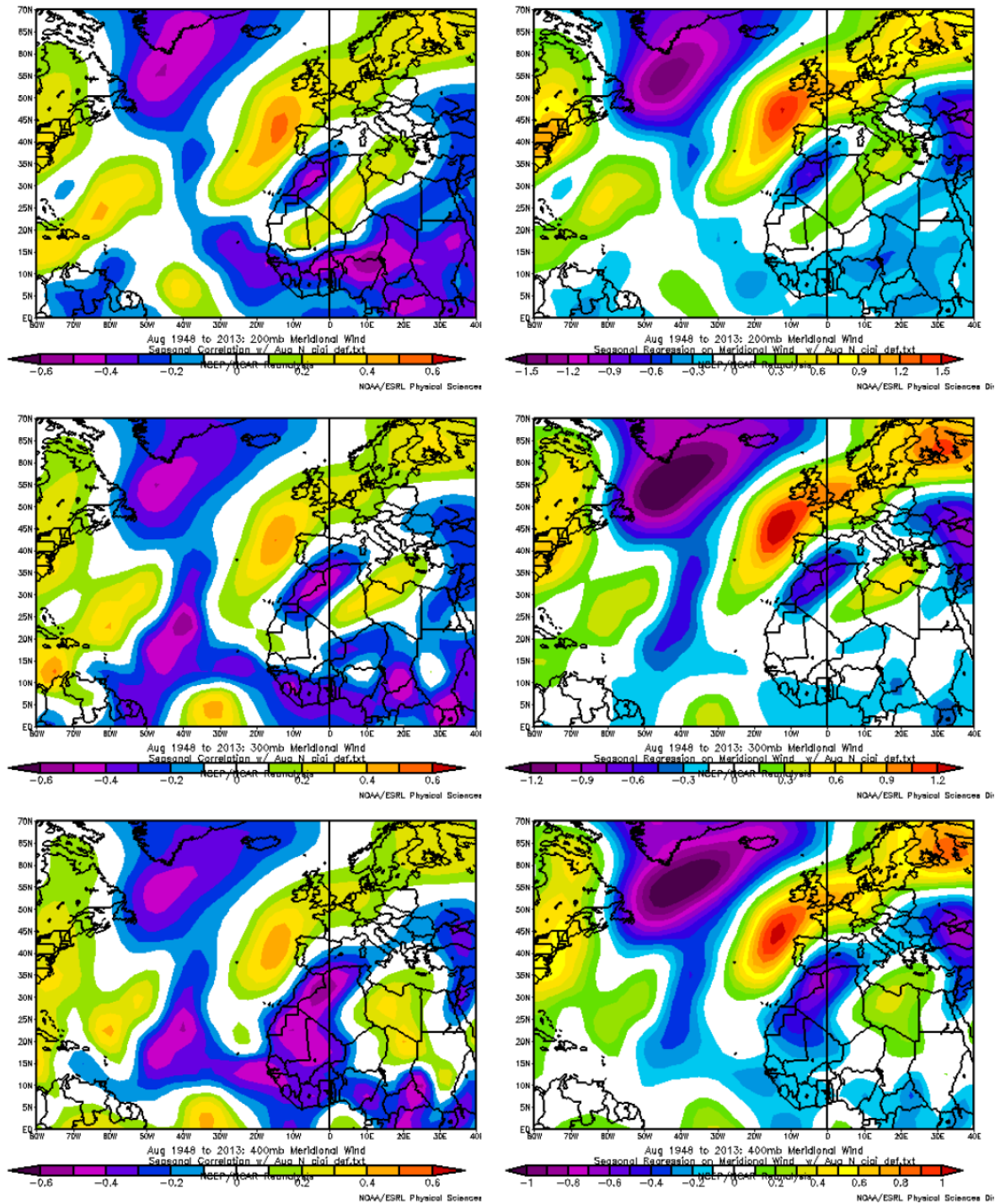
Figure S11-3. NCEP monthly correlation and regression plots between the zonal wind at different pressure levels (400, 500 and 600 hPa) and the monthly NAFDI for August months of the period 1980-2013.



1

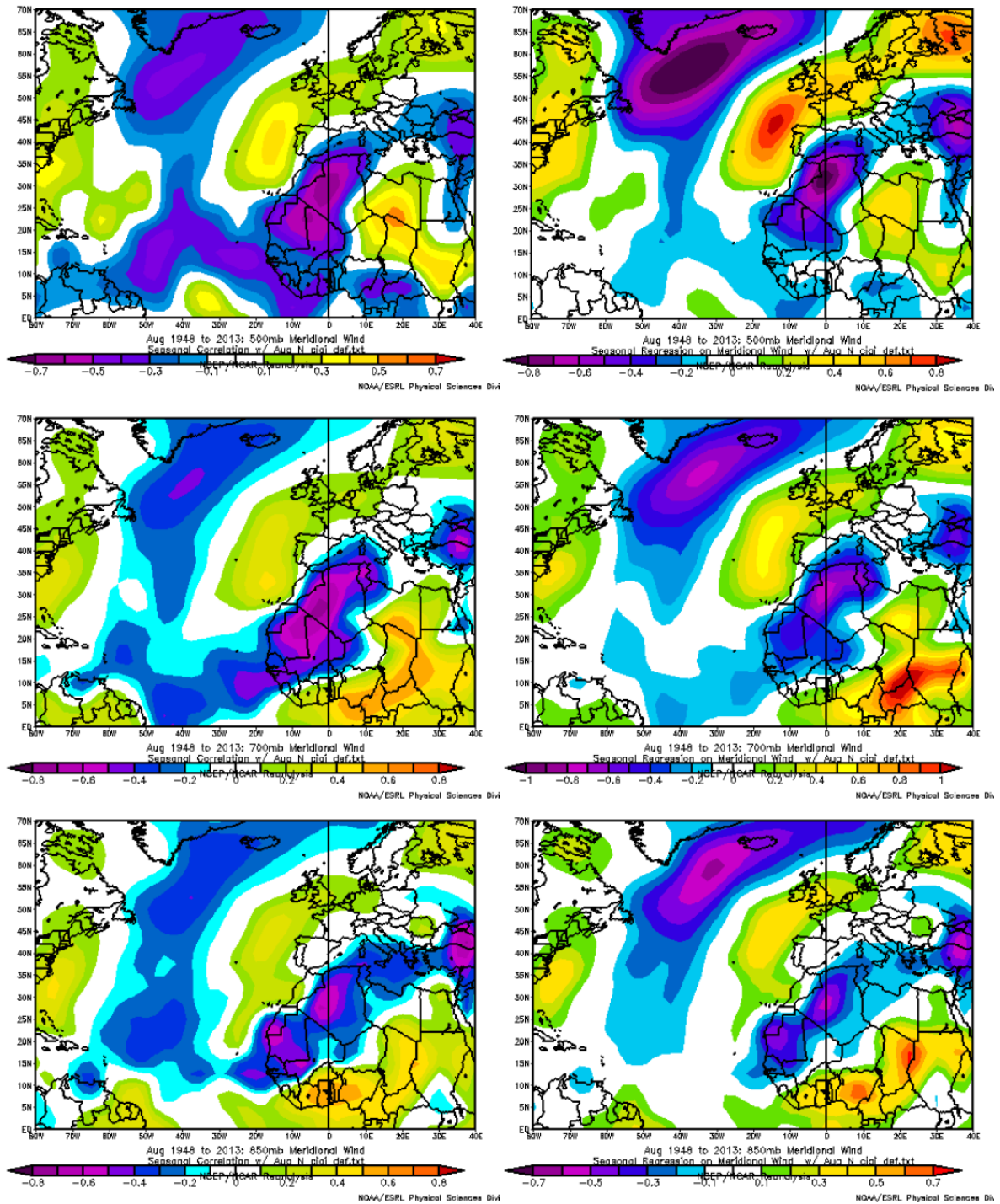
2 Figure S11-4. NCEP monthly correlation and regression plots between the zonal wind at
 3 different pressure levels (700, 850 and 925 hPa) and the monthly NAFDI for August months
 4 of the period 1980-2013.

5



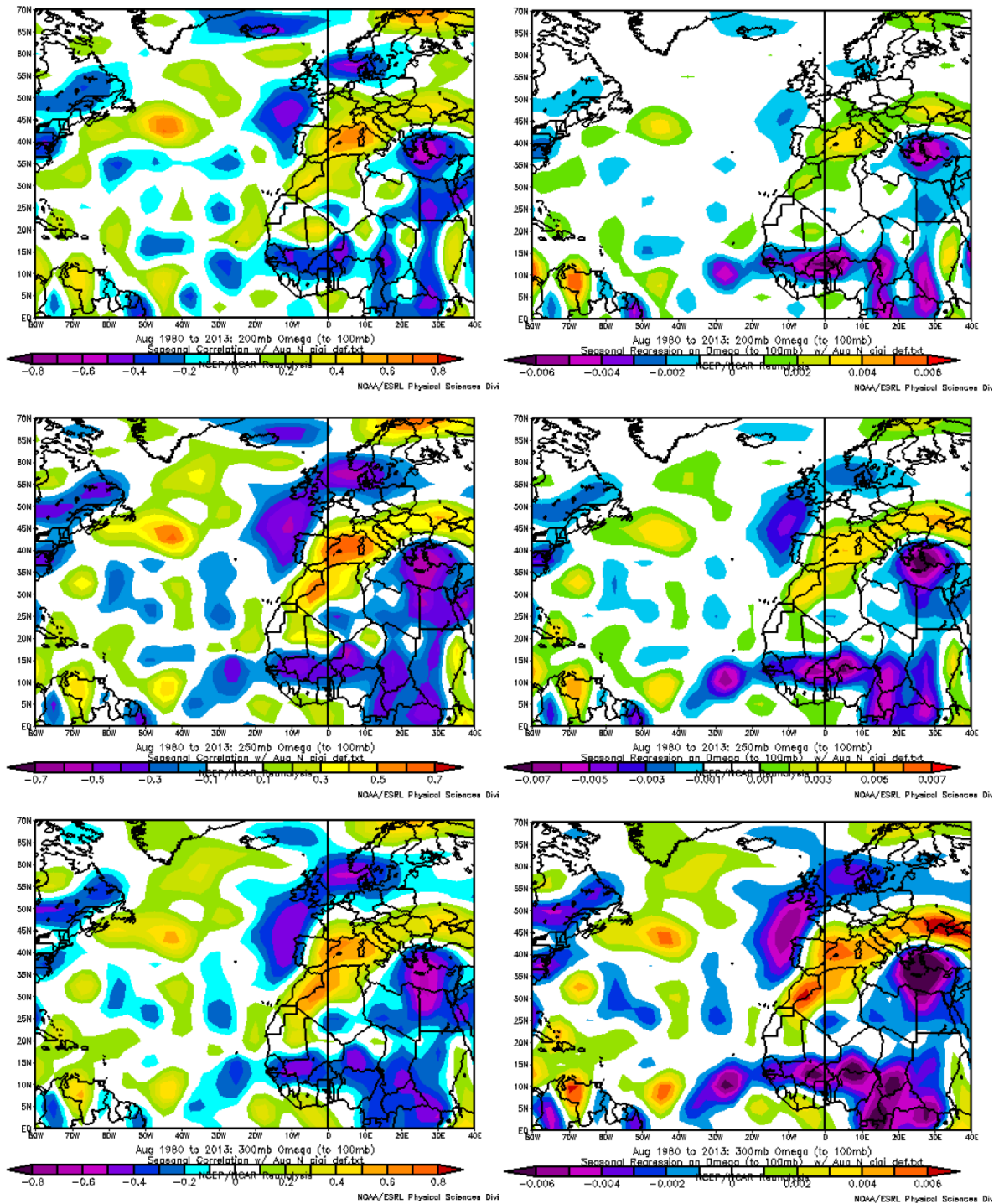
1
 2 Figure S11-5. NCEP monthly correlation and regression plots between the meridional wind at
 3 different pressure levels (200, 300 and 400 hPa) and the monthly NAFDI for August months
 4 of the period 1980-2013.

5



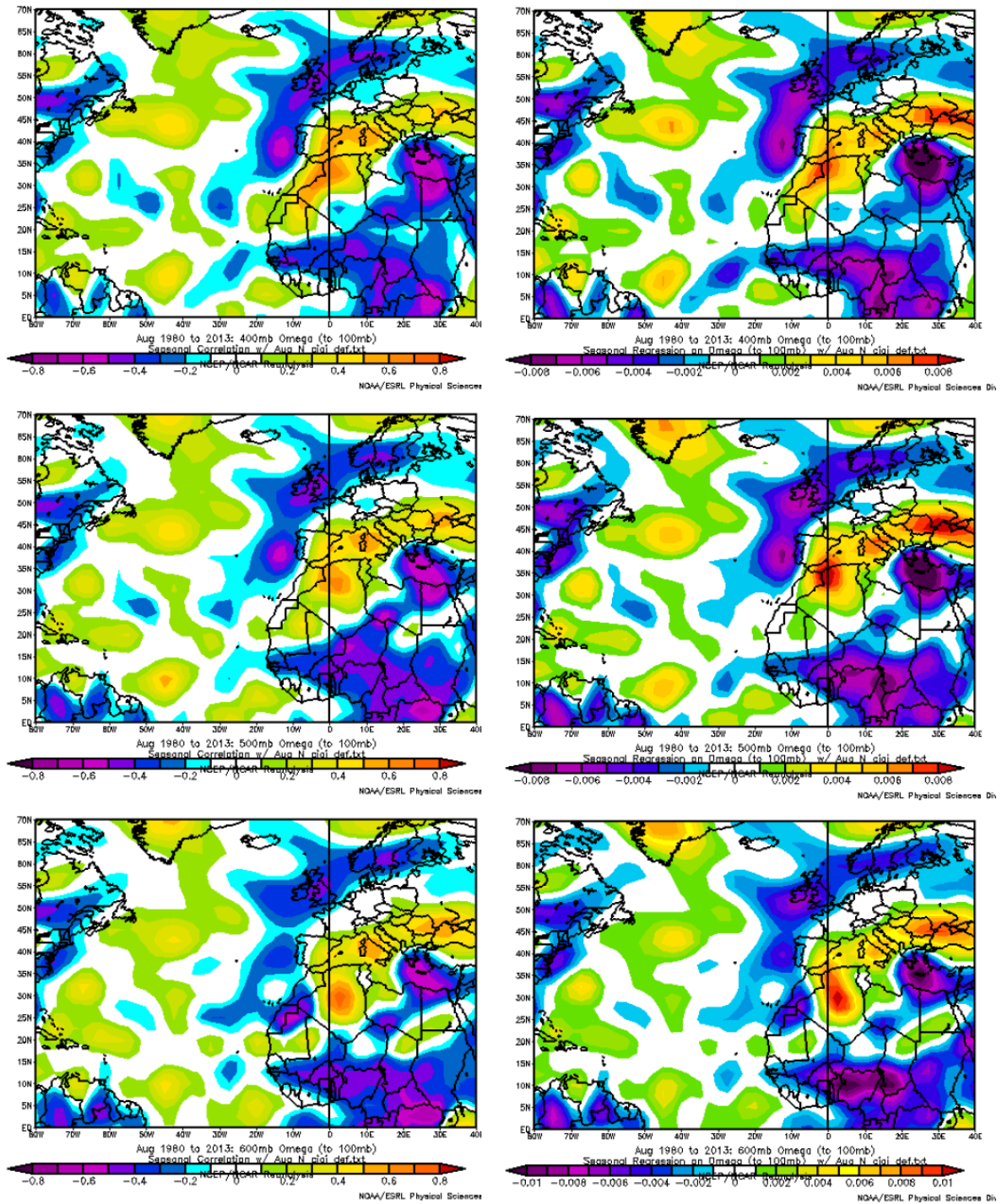
1
 2 Figure S11-6. NCEP monthly correlation and regression plots between the meridional wind at
 3 different pressure levels (500, 700 and 850 hPa) and the monthly NAFDI for August months
 4 of the period 1980-2013.

5



1
 2 Figure S11-7. NCEP monthly correlation and regression plots between the omega at different
 3 pressure levels (200, 250 and 300 hPa) and the monthly NAFDI for August months of the
 4 period 1980-2013.

5



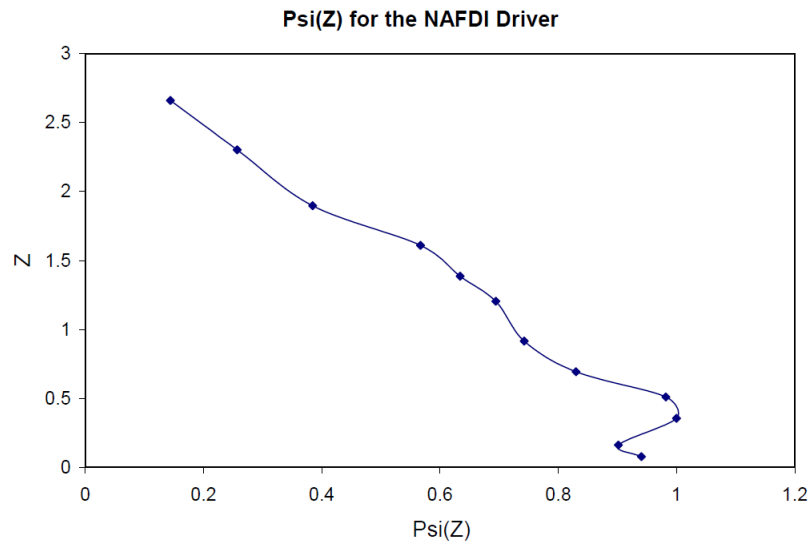
1

2 Figure S11-8. NCEP monthly correlation and regression plots between the omega at different
 3 pressure levels (400, 500 and 600 hPa) and the monthly NAFDI for August months of the
 4 period 1980-2013.

5

6

1 **S12. Vertical structure of the Rossby wave that drives the NAFDI variations**
2 **represented using the variables of Geisler and Dickinson (1975).**



3
4 Figure S12. Vertical structure of the Rossby wave that drives the NAFDI variations
5 represented using the same variables than Geisler and Dickinson (1975), for comparison (they
6 are very similar) with the vertical structure of the external Rossby wave of Geisler and
7 Dickinson (1975) with “effective wavenumber” 10.8 (see their Figure 10).

8
9

1 **S13. Multilinear least-square regression of daily NAFDI as function of ZWA300**
 2 **and O500.**

3 We have performed a multilinear least-square regression of daily NAFDI as function of
 4 ZWA300 and O500 ($NAFDI = BI + BZ*ZWA300 + BO*O500$) for the period 1980-2013 20
 5 June – 17 September. Additionally, we have performed the same regression but for 5-day
 6 running means. These results, shown in Table S13, strongly support the arguments we have
 7 exposed in subsection 3.4.

8

9 Table S13. Details of the multilinear least-square regression of daily NAFDI as function of
 10 ZWA300 and O500 ($NAFDI = BI + BZ*ZWA300 + BO*O500$); and for the same regression
 11 but for 5-day running means.

12

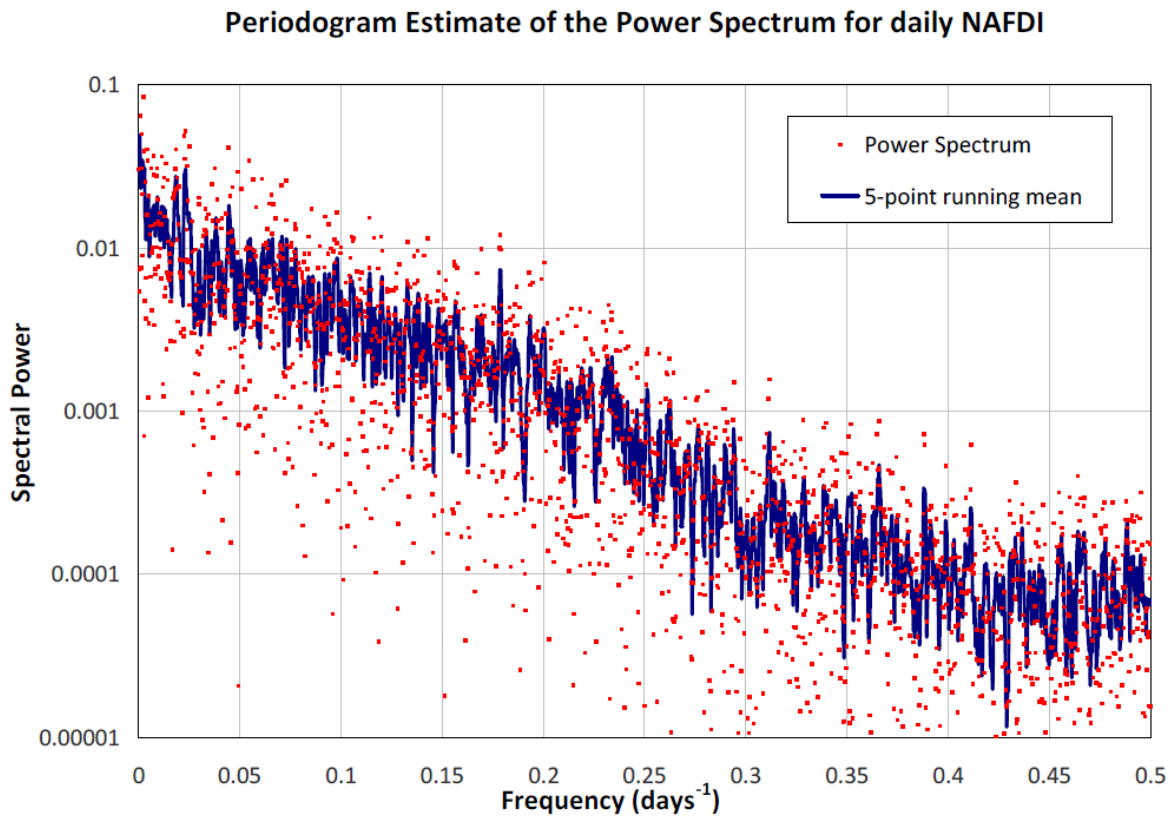
	BI (std.dev)	BZ (std.dev)	BO (std.dev)	Linear correlation	R square	Typical Error
Daily	0.118 (0.041)	0.116 (0.006)	21.1 (0.8)	0.533	0.284	2.25
5-day run. mean	0.074 (0.030)	0.143 (0.005)	29.4 (0.9)	0.656	0.430	1.61

13

14

15

1 **S14. NAFDI power spectra.**



2

3 Figure S14-1. Power spectrum of the daily NAFDI time series for the period 20 June -17
 4 September 1980-2013.

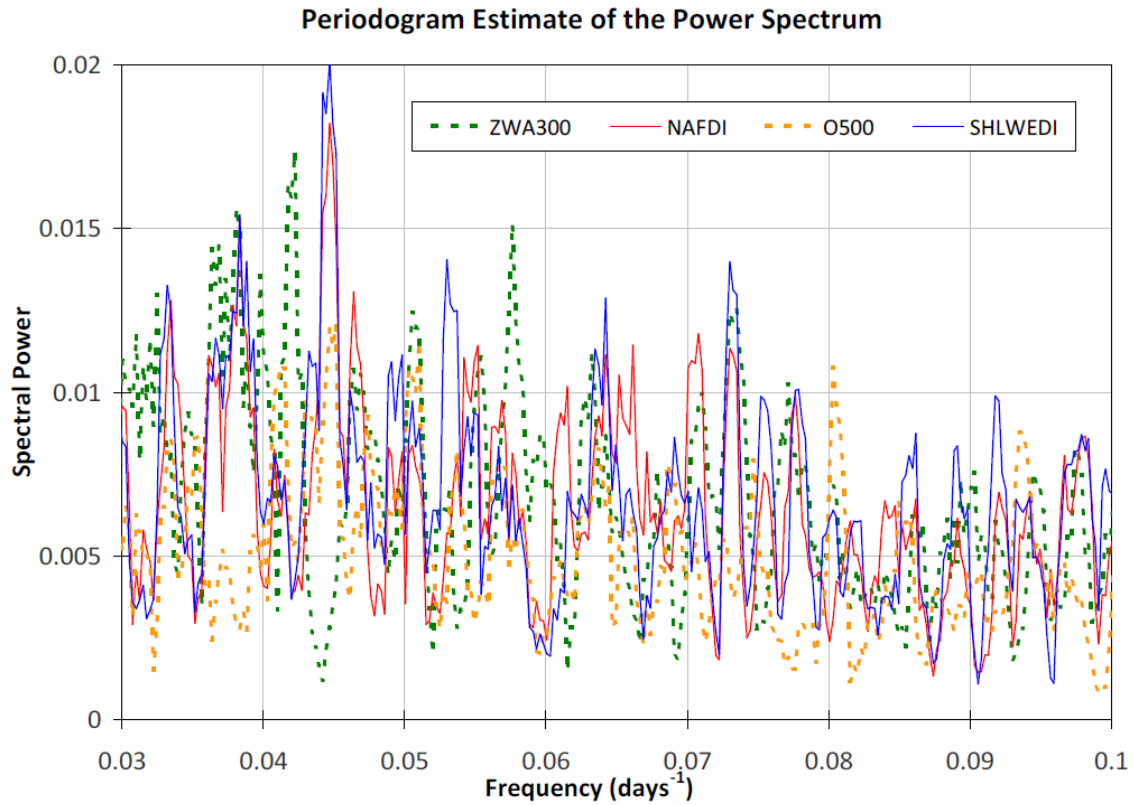
5

Period (P) in days	NAFDI	SHLWEDI	O500	ZWA300	N F
Constant term	0.6%	0.4%	0.4%	0.2%	1
P > 30	37.9%	40.7%	21.8%	34.9%	136
10 ≤ P ≤ 30	33.4%	35.3%	25.7%	34.1%	273
5 ≤ P < 10	20.5%	17.0%	23.5%	20.1%	410
P < 5	7.6%	6.6%	28.6%	10.7%	1229

6 Table S14. Distribution of spectral power in the different frequency ranges (using the period
 7 for indicating the frequency ranges) for the indicated daily time series. “NF” indicates the

1 number of Fourier discrete frequencies in the considered range. The longest period considered
2 is 4096 days (the length of the considered summer time series).

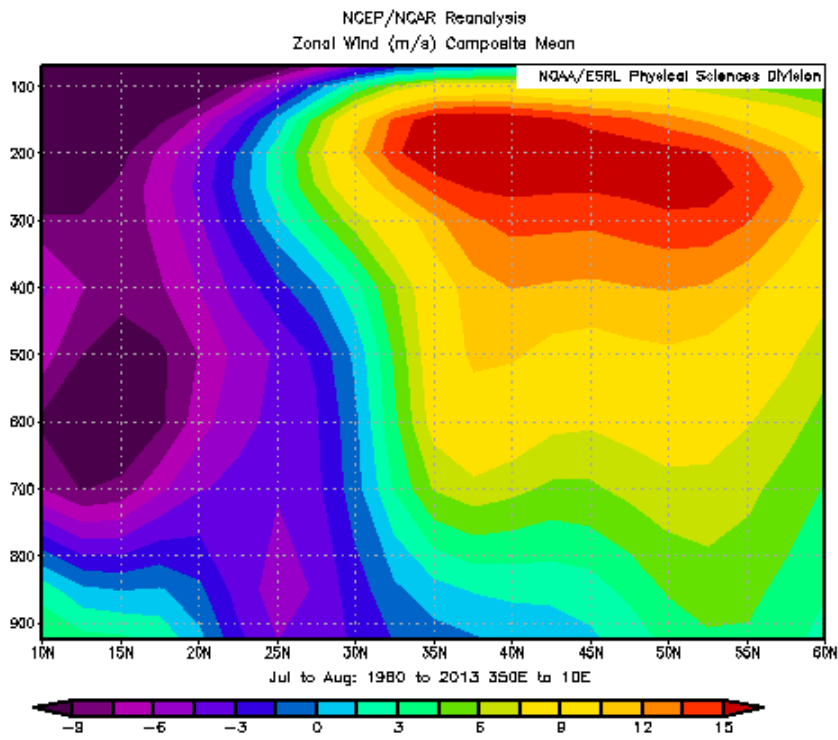
3 Figure S14-2 shows the power spectra of the 4 time series in the intermediate range, after
4 applying a 5-point running mean (note that there are 273 points -discrete Fourier frequencies-
5 in the considered range). The total power of the full spectrum for the SHLWEDI, O500 and
6 ZWA300 time series, has been normalized to that of the NAFDI time series, before plotting
7 the power spectra in Figure S14-2 for easiness in the comparison.



8
9 Figure S14-2. Power spectra of the NAFDI, SHLWEDI, ZWA300 and O500 time series in the
10 intermediate range, after applying a 5-point running mean.

11
12

1 **S15. Mean zonal wind for a latitude-vertical cross-section.**



2

3 Figure S15. Mean zonal wind (averaged also in longitude from 10°W to 10°E) for a latitude-
4 vertical cross-section during the period July-August 1980-2013.

5

6

1 **References**

2 Geisler, J. E., and Dickinson, R. E.: External Rossby modes on a beta-plane with realistic
3 vertical wind shear, *Journal of the Atmospheric Sciences*, 32, 2082-2093, 1975.

4 Holton, J. R.: An introduction to dynamic meteorology, Third edition, International
5 Geophysics Series, vol. 48, Academic Press, San Diego, California, 1992

6 Lavaysse, C., Flamant, C., and Janicot, S.: Regional-scale convection patterns during strong
7 and weak phases of the Saharan heat low, *Atmos. Sci. Lett.*, 11, 255–264,
8 doi:10.1002/asl.284, 2010a.

9 Lavaysse, C., Eymard, L., Flamant, C., Karbou, F., Mimouni, M., and Saci, A.: Monitoring
10 the West African heat low at seasonal and intra-seasonal timescales using AMSU-A sounder.
11 *Atmospheric Science Letters* 14, 263-271, 2013.

12 Lavaysse, C., Flamant, C., Evan, A., Janicot, S., and Gaetani, M.: Recent climatological trend
13 of the Saharan heat low and its impact on the West African climate, *Climate Dyn.*, 715, 1-20,
14 doi:10.1007/s00382-015-2847-z, 2015.

15